Coordination Complexes

International Edition: DOI: 10.1002/anie.201912745
German Edition: DOI: 10.1002/ange.201912745

An Adaptable N-Heterocyclic Carbene Macrocycle Hosting Copper in Three Oxidation States

*Yang Liu, Stefan G. Resch, Iris Klawitter, George E. Cutsail III, Serhiy Demeshko, Sebastian Dechert, Fritz E. Kühn, Serena DeBeer, and Franc Meyer**

Abstract: *A neutral hybrid macrocycle with two trans-positioned N-heterocyclic carbenes (NHCs) and two pyridine donors hosts copper in three oxidation states (+I–+III) in a series of structurally characterized complexes (**1–3**). Redox interconversion of $[LCu]^{+/2+/3+}$ is electrochemically (quasi)-reversible and occurs at moderate potentials ($E_{1/2} = -0.45$ V and +0.82 V (vs. Fc/Fc^+)). A linear C^{NHC}-Cu-C^{NHC} arrangement and hemilability of the two pyridine donors allows the ligand to adapt to the different stereoelectronic and coordination requirements of Cu^I versus Cu^{II}/Cu^{III}. Analytical methods such as NMR, UV/Vis, IR, electron paramagnetic resonance, and Cu Kβ high-energy-resolution fluorescence detection X-ray absorption spectroscopies, as well as DFT calculations, give insight into the geometric and electronic structures of the complexes. The XAS signatures of **1–3** are textbook examples for Cu^I, Cu^{II}, and Cu^{III} species. Facile 2-electron interconversion combined with the exposure of two basic pyridine N sites in the reduced Cu^I form suggest that $[LCu]^{+/2+/3+}$ may operate in catalysis via coupled $2e^-/2H^+$ transfer.*

Introduction

Copper complexes attract significant interest because of their various applications as catalysts in organic transformations such as C–C/X bond formation and C–H bond activation reactions, and also for their involvement in biological oxidation and oxygenation processes.[1,2] These copper-mediated reactions generally exploit oxidation state changes of the metal ion, and proposed mechanistic scenarios primarily involve the Cu^I/Cu^{II} or Cu^I/Cu^{III} couples. However, in contrast to numerous examples of organometallic copper(I) and copper(II) complexes, organocopper(III) species have rarely been isolated and authenticated because of their limited stability.[1d,3,4] The majority of recently reported organocopper(III) complexes are stabilized by anionic C/N-based macrocycles, such as Ribas's[4a] triazamacrocycles, Wang's[4b] azacalix[1]arene[3]pyridines, Furuta's[4c,d,i] N-confused porphyrins/corroles, and Srinivasan's[4g] biphenyl-embedded porphyrinoides (Figure 1a). In all the aforementioned complexes, the formally Cu^{III} ion adopts a square planar coordination geometry. However, the assignment of the physical oxidation states of copper—especially when ligated by redox non-innocent ligands—should be considered with caution.[5] For example, it was recently suggested that the formally $3d^8$ Cu^{III} species $[Cu(CF_3)_4]^-$ features an inverted ligand field and that it is best described as having a $3d^{10}$ Cu^I electronic configuration.[5a,b,d] In such ambiguous cases, the

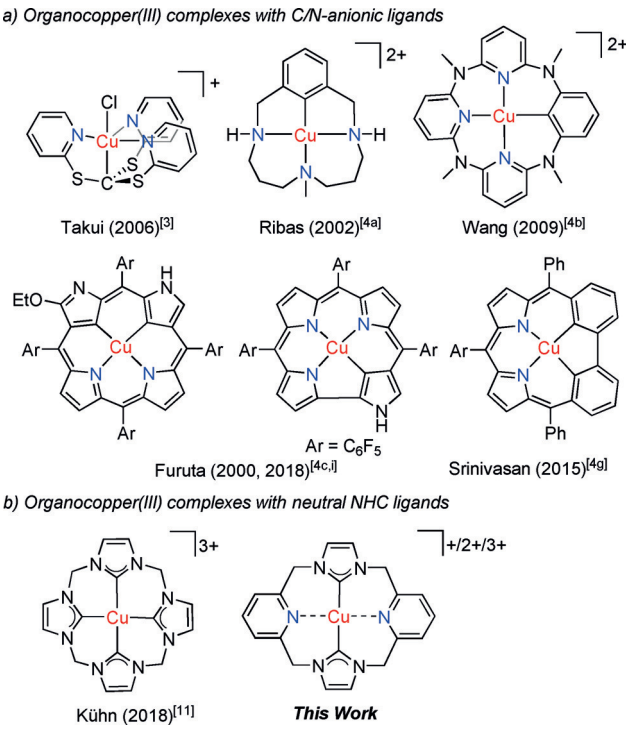

Figure 1. Examples of previously reported organocopper(III) complexes.

[*] Dr. Y. Liu, Dr. S. G. Resch, Dr. I. Klawitter, Dr. S. Demeshko, Dr. S. Dechert, Prof. Dr. F. Meyer
Institute of Inorganic Chemistry, University of Göttingen
Tammannstrasse 4, 37077 Göttingen (Germany)
E-mail: franc.meyer@chemie.uni-goettingen.de
Dr. G. E. Cutsail III, Prof. Dr. S. DeBeer
Department of Inorganic Spectroscopy
Max Planck Institute for Chemical Energy Conversion
Stiftstrasse 34–36, 45470 Mülheim an der Ruhr (Germany)
Prof. Dr. F. E. Kühn
Department of Chemistry & Catalysis Research Center
Technische Universität München
Lichtenbergstrasse 4, 85748 Garching bei München (Germany)
Supporting information and the ORCID identification number(s) for the author(s) of this article can be found under: https://doi.org/10.1002/anie.201912745.

combination of K-edge X-ray absorption spectroscopy (XAS) and theoretical calculations is a useful toolbox for assigning oxidation states.[5,6]

Over the last decades, N-heterocyclic carbenes (NHCs) have become one of the most popular ligand classes in organometallic chemistry and catalysis.[7] As a consequence of their strong σ-donating and variable π-accepting abilities, NHCs are capable of supporting metal complexes in a range of oxidation states, and they are now emerging as useful scaffolds for the stabilization of 3d metal ion species in high oxidation states.[8]

NHC-copper chemistry has developed rapidly since the first NHC-Cu^{I} complex $[(NHC)_2Cu][OTf]$ was reported in 1993 by Arduengo.[9,10] To date, numerous examples of Cu^{I} complexes are known, and they usually adopt a linear geometry that is common to d^{10} coinage metal ions. In contrast, NHC-ligated Cu^{II} complexes are much rarer,[8] and a single NHC-Cu^{III} complex has been authenticated; the latter is based on a rigid tetra(N-heterocyclic) carbene macrocycle (Figure 1b) and is the only organocopper(III) complex of a neutral ligand reported to date.[11]

Most of the reported NHC-Cu^{II} complexes require appended chelating N- or O-donors, and they often contain anionic co-ligands.[12] The groups of K. Meyer and J. Long prepared two examples of Cu^{II} complexes with neutral N-anchored tripodal tris(NHC) or NHC-bridged polypyridyl ligands, respectively.[13] Several computational studies suggested the existence of NHC-Cu^{III} species during carbene-halide/aryl reductive elimination and oxidative coupling of carbenes,[14] but such intermediates have so far eluded isolation. The seminal tetra(NHC)-Cu^{III} complex shown in Figure 1b was synthesized by a disproportionation reaction starting from the corresponding tetra(imidazolium) salt and $Cu_2(OAc)_4$, and it shows the square planar coordination geometry expected for a low-spin d^8 ion.[11] However, details on its electronic structure and valence state were not reported. Furthermore, in this case, as well as in most Cu^{III} systems reported to date, the drastically different coordination geometry preferences for Cu^{I} versus Cu^{II} and Cu^{III} prevented any reversible redox shuttling between the different oxidation states, because redox changes are usually accompanied by major structural changes. Accordingly, the Cu^{I} complex of Kühn's tetra(NHC) macrocycle, obtained when using CuOAc as the copper source, exhibits a tetranuclear structure composed of two tetra(NHC) ligands and four linearly coordinated Cu^{I} ions.[11]

To circumvent major structural rearrangements or changes in nuclearity during redox interconversion and allow for isolation of the Cu-NHC system in three oxidation states from Cu^{I} to Cu^{III}, we have exploited the concept of ligand hemilability in a macrocyclic NHC/pyridine hybrid scaffold. This system can adapt to the different metal ion coordination environments required (Figure 1b). A number of bi-, tri-, tetra-, and penta-dentate cyclic or acyclic NHC/pyridine hybrid ligands have previously been introduced in organometallic chemistry,[7c,13b,15] as these may favorably combine the strong *σ*-donor properties of NHCs with the relatively weak *σ*-N-donor character of pyridine groups. Among them, the macrocyclic ligand derived from $[H_2L][PF_6]_2$ (Scheme 1) with two *trans* disposed NHC moieties and two pyridine moieties has been utilized for the synthesis of Ni^{II} and Fe^{II} complexes.[15a,d] The latter can be further oxidized to the corresponding Fe^{III} congener, indicating the ability of this ligand to stabilize higher valent metal complexes.

Herein we report a series of copper complexes in oxidation states +I, +II, and +III that can be (quasi)reversibly interconverted at moderate potentials. The copper ion is hosted within the neutral macrocyclic bis(NHC)-bis(pyridine) ligand framework (L) throughout the series, and a suite of experimental methods (XRD, variable-temperature (VT) NMR, XAS, absorption, superconducting quantum interference device (SQUID) magnetometry, and electron paramagnetic resonance (EPR) spectroscopy), as well as DFT calculations, have been employed to elucidate the geometric and electronic structures of the three complexes. To the best of our knowledge, this is the first system that can stabilize copper complexes in all three relevant oxidation states (+I, +II, and +III) within a single host scaffold, and without undergoing major structural changes.

Results and Discussion

Copper(I) complex and its dynamics. The copper(I) complex [LCu][PF_6] (**1**) can be readily synthesized via two independent routes with good isolated yields (ca. 66%). The complex is obtained either by reaction of the bis(imidazolium) salt $[H_2L][PF_6]_2$ with mesitylcopper (MesCu, 2.0 equiv) in acetonitrile (MeCN) or by initial deprotonation of $[H_2L][PF_6]_2$ with $K[N(SiMe_3)_2]$ (2.0 equiv) followed by treatment with $[Cu(NCMe)_4][PF_6]$ (1.0 equiv) in MeCN (Scheme 1). A yellow precipitate is generated in both reactions after long periods of reaction (1 week). **1** is isolated as a yellow powder after simple filtration. The electrospray ionization mass spectrum (ESI-MS) of a MeCN solution of this yellow powder is dominated by a peak at $m/z = 405.1$ amu

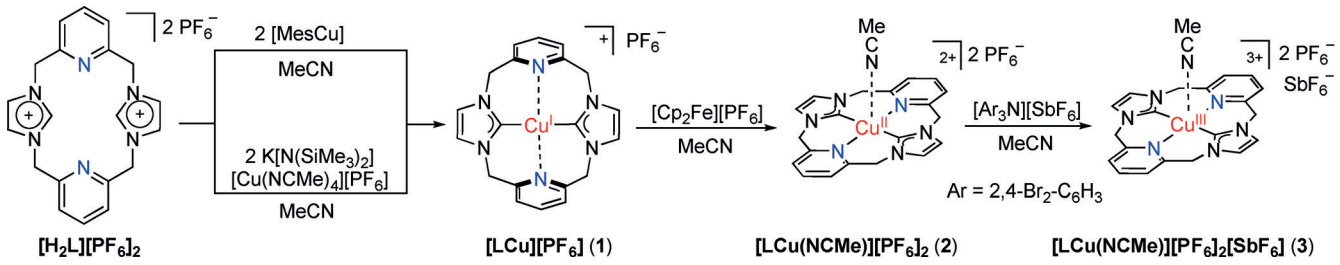

Scheme 1. Synthesis of the Cu^{I}, Cu^{II}, and Cu^{III} complexes of the NHC/pyridine hybrid macrocycle L.

characteristic for the cation $[LCu]^+$ (Supporting Information, Figure S10), supporting the formation of the desired product $[LCu][PF_6]$.

At room temperature, complex **1** is stable both in the solid state and in MeCN solution under an inert atmosphere. However, it slowly decomposes in MeCN solution under air, as evidenced by UV/Vis monitoring (Figure S6). Interestingly, slow diffusion of Et_2O into a saturated MeCN solution of the crude yellow powder yields not only the mononuclear complex **1** as yellow crystals in a large amount, but also a few colorless crystals of a different compound that turned out to be the dinuclear complex $[L_2Cu_2][PF_6]_2$ (**1′**). The structures of both **1** and **1′** were determined by X-ray diffraction and are depicted without their anions in Figure 2 and Figure S2, respectively. In the minor product **1′**, two macrocycles L are bridged by two Cu^I ions that are both ligated linearly by two NHC donors from the different ligands. This structural motif has previously been seen for the silver(I) and gold(I) analogues, $[L_2Ag_2][PF_6]_2$[16] and $[L_2Au_2]Br_2$,[17] and resembles the structure of a dinuclear copper(I) complex $[L^{Ph\text{-}NHC}{}_2Cu_2][PF_6]_2$ with a related bis(NHC) macrocycle lacking additional pyridine N donors.[18] When dissolved in MeCN or acetone, **1′** immediately converts into the monomeric form **1**, even at low temperatures, as evidenced by ^{1}H NMR and ESI-MS analysis (Supporting Information). This suggests a fast equilibrium between **1** and **1′** in solution that lies far on the side of mononuclear **1** in the above polar solvents.

In the major product **1**, the metal ion is hosted within the macrocyclic cavity and is bound to the two NHC donors in a quasi-linear geometry (C^{NHC}-Cu-C^{NHC}: 169.6(1)°). The Cu–C^{NHC} bond lengths of 1.939(2) Å and 1.946(2) Å agree with reported values for Cu^I–NHC complexes.[11,19,20] The two pyridine rings adopt a near-orthogonal orientation with respect to the plane defined by the two C^{NHC} and the two pyridine N atoms, with interplanar angles of 78.6(1)° and 69.7(1)°, respectively. Furthermore, the distances between the pyridine N atoms and the central Cu^I ion (2.496(2) Å and 2.706(2) Å) are substantially longer than the Cu···N^{py} distances in other reported NHC-Cu^I complexes with ancillary pyridine donors,[21] though comparable to those in $[(It\text{Bu}^{CNC})_2Cu_2][PF_6]_2$ (2.422(2)–2.830(2) Å; $It\text{Bu}^{CNC}$ is a tridentate pyridine-bridged dicarbene ligand);[22] the N^{py}···Cu···N^{py} angle in **1** is 164.5(1)°. These structural features indicate weak interactions at best, in accordance with the preference of linear geometry of Cu^I–NHC complexes. However, weak Cu···py interactions may contribute to the predominance of the monomeric species **1** (see proceeding text) and the deviation of the C^{NHC}-Cu-C^{NHC} angle (169.6°) from linearity.

The mononuclear structure of **1** contrasts with the structures of the corresponding Ag^I and Au^I complexes of the hybrid macrocycle L, and the Cu^I complex of a related macrocycle lacking the pyridine N donors, which were shown to exist as dinuclear or even tetranuclear ($[L_2Ag_4][PF_6]_4$) complexes in the solid state, with linearly coordinated metal ions bound to NHC or pyridine donors from two different macrocycles.[16–18,23] Dinuclear or tetranuclear structural motifs ($[L^{NHC}Cu_2]I_2$,[20] $[L^{NHC}{}_2Cu_4][PF_6]_4$[11]) have also been observed for copper(I) complexes of macrocyclic tetracarbene ligands. In iron complexes $[LFe^{II}(NCMe)_2][PF_6]_2$[15d] and $[LFe^{III}(NCMe)_2][PF_6]_3$,[15d] as well as in the nickel complex $[LNi^{II}]Br_2$,[15a] the macrocyclic ligand L binds as a typical tetradentate $C^{NHC}{}_2N^{py}{}_2$ donor with the Fe–N^{py} and Ni–N^{py} bonds along the planes of the pyridine rings; the macrocycles are severely puckered and *trans*-located imidazol-2-ylidene rings are twisted with respect to each other. In complex **1**, the two imidazol-2-ylidene rings are almost coplanar (Figure 2 a).

In agreement with the crystallographic structure and the proposed weak interaction of the pyridyl groups with the metal center, the ^{15}N NMR resonance of N^{py} in **1** is shifted only slightly to lower field (−67.5 ppm) compared to the ligand precursor $[H_2L][PF_6]_2$ (−77.6 ppm). The ^{13}C NMR spectrum exhibits a down-field shift of the signal for the carbene C from 153.9 ppm in $[H_2L][PF_6]_2$ to 177.4 ppm in **1**, which is characteristic of NHC-Cu^I complexes.[11,20,21] However, the simplicity of the room-temperature ^{1}H NMR spectrum of **1** (in $[D_3]$MeCN), displaying a singlet at 5.20 ppm for the macrocyclic CH_2 linkers and one set of signals for the pyridyl rings, suggests a highly dynamic behavior in solution with apparent D_{2h} symmetry of the complex on the NMR timescale. We attribute this to a flipping of the pyridyl rings via a process in which these rings become coplanar with the macrocyclic core and the Cu···N^{Py} vector. DFT computations indicate such a conformation in which one of the pyridine rings has become coplanar with the macrocycle, reflecting the pyridine ring flip, to be only 8.2 kcal mol^{-1} higher in energy (Figure S47).

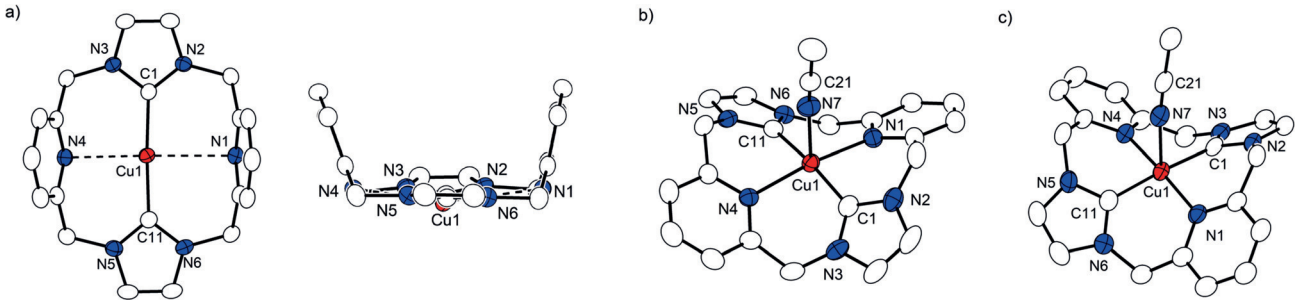

Figure 2. a) Molecular structures of **1** (left, upside view; right, frontside view), b) **2**, and c) **3** (only one of the two crystallographically independent molecules in the asymmetric unit is shown), with 50% probability ellipsoids. Hydrogen atoms, lattice solvent (MeCN), and anions are omitted for clarity. Selected atom distances and angles of **1**, **2**, and **3** are listed in Table 1.

Similar diffusion coefficients of the imidazolium salt $[H_2L][PF_6]_2$ ($D_{298K} = 1.05 \times 10^{-9}\ m^2 s^{-1}$) and **1** ($D_{298K} = 1.17 \times 10^{-9}\ m^2 s^{-1}$) derived from ^1H diffusion ordered spectroscopy (DOSY) experiments support that the complex remains mononuclear with a 1:1 metal:ligand ratio in solution. The dynamic behavior of **1** in solution was probed by VT ^1H NMR experiments in [D$_6$]acetone (Figure 3; Figures S39,S40).

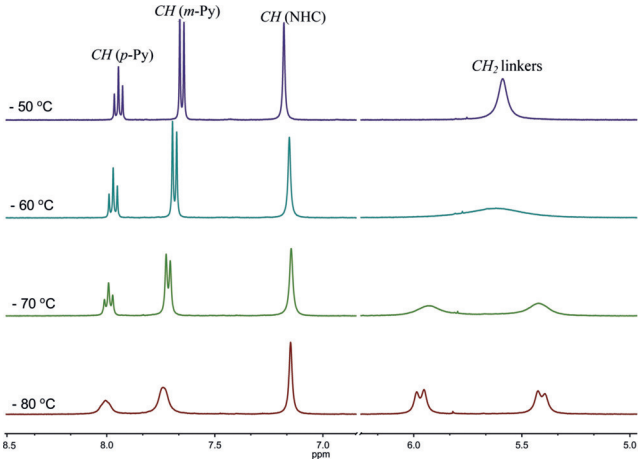

Figure 3. VT ^1H NMR spectra for **1** in [D$_6$]acetone (only regions 5.0–6.3 ppm and 6.8–8.5 ppm are shown for clarity).

Upon decreasing the temperature, signals arising from the pyridine groups and the imidazol-2-ylidene backbone shift slightly to lower and higher field, respectively (Figure S39), and become broad at −80 °C. The peak for the CH_2 linkers exhibits a significant down-field shift ($\Delta\delta = 0.23$ ppm) that begins to broaden at −50 °C and finally splits into a pair of apparent doublets at −80 °C (coalescence temperature $T_c = -62$ °C, $\Delta G^{\ddagger} = 9.5$ kcal mol^{-1}), with a coupling constant of $J_{ab} = 13.6$ Hz that is typical for geminal coupling (Figure 3; Figure S40). This suggests that flipping of the pyridyl rings becomes slow on the NMR timescale at low temperatures. The activation energy ($E_a = 17.8$ kcal mol^{-1}) and parameters ($\Delta H^{\ddagger} = 17.4$ kcal mol^{-1} and $\Delta S^{\ddagger} = 37.2$ cal mol^{-1} K^{-1}) for this process were derived from Arrhenius and Eyring analyses of the VT NMR data (Figures S44,S45). The possible C_{2v} and C_{2h} symmetric isomers of **1** (with the two pyridine rings directed towards the same or opposite sides, respectively) are almost isoenergetic according to DFT calculations (Figure S47); broadening of all ^1H NMR signals at low temperatures may reflect the presence of both isomers exhibiting very similar NMR shifts.

In contrast, the ^1H NMR spectra of related iron(II) and nickel(II) complexes in which L binds as a tetradentate $C^{NHC}{}_2N^{py}{}_2$ ligand, $[LFe^{II}(NCMe)_2][PF_6]_2$[15d] and $[LNi^{II}]Br_2$,[15a] reveal a pair of doublets for the CH_2 linkers at room temperature because of restricted flexibility of the puckered macrocycle. Compared with activation parameters for the conformational ring inversion in $[LFe^{II}(NCMe)_2][PF_6]_2$ ($\Delta H^{\ddagger} = 15.1$ kcal mol^{-1}, $\Delta S^{\ddagger} = -4.7$ cal mol^{-1} K^{-1})[15d] or in $[L^aFe(CH_3CN)][PF_6]_2$ (L^a = acyclic tetradentate bis(NHC)-bis(pyridine) ligand; $\Delta H^{\ddagger} = 14.4$ kcal mol^{-1}, $\Delta S^{\ddagger} = -0.2$ cal mol^{-1} K^{-1}),[24] the large and positive activation entropy in case of complex **1** indicates a different dynamic process with a more disordered transition state, which is attributed to the pyridyl ring flip. Complex $[LNi^{II}]Br_2$ with square planar coordination geometry of the low-spin d^8 nickel(II) shows a stationary puckered conformation and no ring inversion dynamics on the NMR timescale, even at 80 °C.[15a]

Redox Properties and (Spectro)electrochemistry. The redox properties of **1** were examined by electrochemical methods. Cyclic voltammetry (CV) of **1** in MeCN reveals two redox events at potentials of −0.45 V and +0.82 V ($E_{1/2}$, vs. Fc/Fc$^+$, Figure 4) assigned to the Cu^I/Cu^{II} and Cu^{II}/Cu^{III}

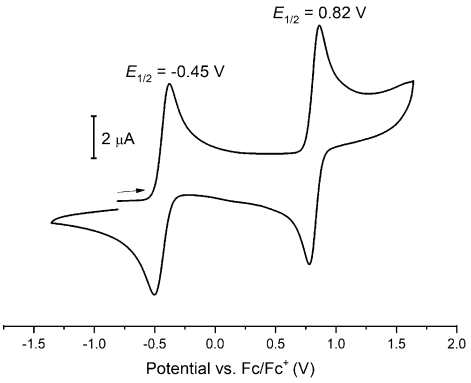

Figure 4. Cyclic voltammogram (100 mV s^{-1}) of complex **1** in MeCN (0.1 M [nBu$_4$N][PF$_6$]) at room temperature.

couples, respectively. The second process is reversible, as judged by the linear dependence of the current on the square root of the scan rate (Randles–Sevcik equation), the similar peak currents of forward and reverse scans ($I_{rp}/I_{fp} = 0.92$), and the peak-to-peak separation ($\Delta E^p = 80$ mV) that is very similar to that of the Fc/Fc$^+$ couple ($\Delta E^p = 76$ mV) under the same conditions (Supporting Information). ΔE^p for the Cu^I/Cu^{II} couple is slightly larger ($\Delta E^p = 124$ mV, $I_{rp}/I_{fp} = 0.86$), likely because it involves some more significant reorganization associated with the movement of the pyridine rings and a planarization of the structure upon oxidation to Cu^{II}. For comparison, the copper complexes $[Cu(I(R)^{CNC})][PF_6]$ (where $I(R)^{CNC}$ is a pincer-type bis(NHC)pyridine ligand; R = Me, Et, and iPr)[21b] and $[(TIMEN^{tBu})Cu][PF_6]$[13a] ($TIMEN^{tBu}$ is a N-anchored tripodal tetradentate tris(NHC) ligand) showed reversible Cu^I/Cu^{II} couples at much higher potential ($E_{1/2}$ in the range +0.02–+0.11 V vs. Fc/Fc$^+$), while a macrocyclic tetra(NHC) ligand (Figure 1b) leads to an irreversible Cu^I/Cu^{II} couple at very negative potential (cathodic peak potential −1.14 V at 100 mV s^{-1}; vs. Fc/Fc$^+$) and an only partially reversible Cu^{II}/Cu^{III} couple at $E_{1/2} = -0.75$ V (vs. Fc/Fc$^+$).[11] Notably, the Cu^{II}/Cu^{III} potential of complex **1** is higher than that of many previously reported Cu^{II} or Cu^{III} complexes with ancillary anionic N- or C-donor ligands.[4a,f,i] The mostly reversible redox behavior of **1** indicates that the macrocyclic NHC-pyridine hybrid ligand L has sufficient structural and electronic flexibility to accommodate copper in all three oxidation states from Cu^I to Cu^{III}.

The sequential oxidation of **1** to the Cu^{II} (**2**) and Cu^{III} (**3**) species yielded characteristic electronic absorption changes as probed by UV/Vis spectroelectrochemistry (UV/Vis-SEC; Figure 5). The UV/Vis spectrum of complex **1** shows two prominent bands at 280 nm ($\varepsilon = 13\,600\ M^{-1}cm^{-1}$) and 340 nm ($\varepsilon = 5000\ M^{-1}cm^{-1}$) that can be assigned to $Cu^{I}\rightarrow$ligand charge transfer transitions (metal-to-ligand, MLCT) based on time-dependent density functional theory (TD-DFT) calculations (B3LYP/tzvp; Figures S5,S48; Supporting Information, Table S5; calculated λ_{max}(calc) = 271 nm and 374 nm). Upon bulk oxidation at 0.8 V (vs. Ag wire), both absorptions at 280 and 340 nm of **1** vanish and two lower intensity bands at 370 nm (shoulder, $\varepsilon = 220\ M^{-1}cm^{-1}$) and 490 nm ($\varepsilon = 120\ M^{-1}cm^{-1}$) emerge corresponding to the Cu^{II} complex formation. This is in line with the observed color change from yellow to red. A clear isosbestic point at 440 nm indicates a single-step conversion without intermediate step(s). The 370 nm feature of **2** largely originates from a ligand→$Cu^{II}(d_{x^2-y^2})$ charge transfer (ligand-to-metal, LMCT) and the 490 nm feature is from a Cu^{II} based d–d transition ($d_{yz}\rightarrow d_{x^2-y^2}$), based on the TD-DFT results (Figure S49, Table S6; λ_{max}(calc) = 335 nm and 452 nm). Upon further electrolysis at 1.5 V (vs. Ag wire), absorptivity increases and the two bands of in-situ-generated **2** are replaced by three more intense bands at 300, 350, and 530 nm, which is indicative of formation of the Cu^{III} complex **3** and consistent with a color change from red to dark-red. TD-DFT calculations assign all these three bands as ligand→Cu^{III} charge transfer transitions (LMCT; Figure S50, Table S7; λ_{max}(calc) = 310, 376, and 512 nm). All spectral changes are fully reversible upon re-reduction. The results of the (spectro)electrochemical studies suggest that preparation of the oxidized copper complexes by chemical bulk oxidation, and their isolation, should be feasible.

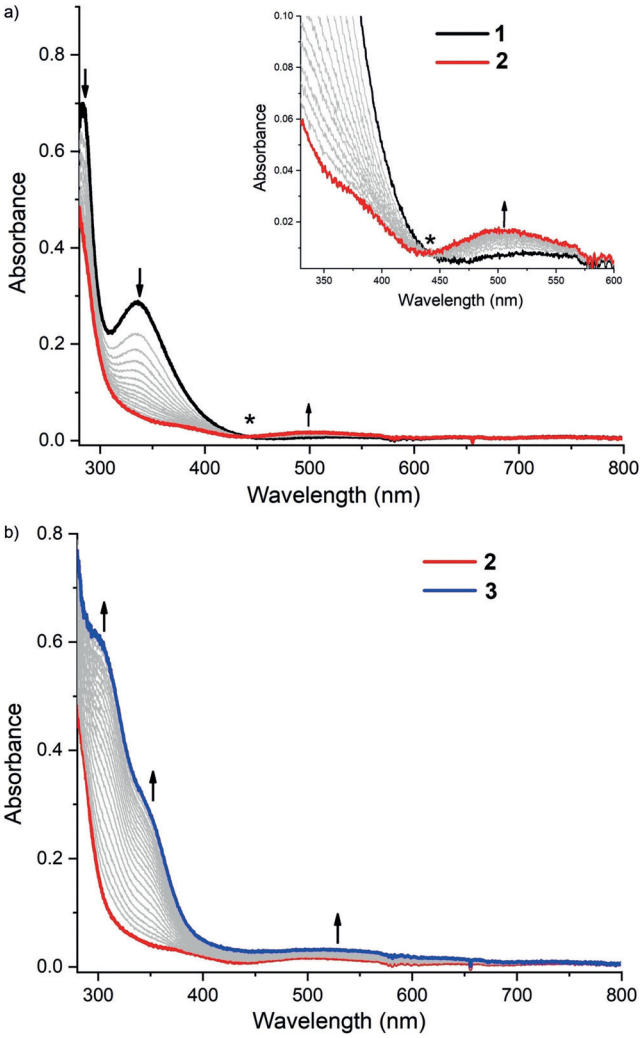

Figure 5. UV/Vis (spectro)electrochemistry showing the continuous oxidation of a) **1** to **2** (at 0.8 V vs. Ag wire; **1** (black), **2** (red); the inset shows a magnified view of the 330–600 nm range) and b) from **2** to **3** (at 1.5 V vs. Ag wire; **2** (red), **3** (blue)) in an MeCN solution containing 0.1 M [nBu$_4$N][PF$_6$]. The isosbestic point is marked with an asterisk.

Copper(II) complex. Using [Cp$_2$Fe][PF$_6$] as oxidant, the Cu^{II} complex [LCu][PF$_6$]$_2$ (**2**) is readily obtained as a red solid in high yield (ca. 86 %) (Scheme 1). An ESI mass spectrum of a MeCN solution of this red solid shows dominant peaks at m/z = 550.1 amu and 202.2 amu, which are characteristic of the monocation $[LCu(PF_6)]^+$ and the dication $[LCu]^{2+}$, respectively (Figure S11). Complex **2** is insensitive to air and moisture over prolonged times, both in solution and in the solid state.

Red block crystals of **2** were obtained by slow diffusion of Et$_2$O into a saturated MeCN solution of the crude material. The molecular structure of the cation of **2** shows that the Cu^{II} ion is five coordinate in the solid state with the tetradentate L establishing a square planar donor environment (C_2N_2 donor set, sum of angles around Cu is 358.0°) and a MeCN ligand occupying an apical position at rather long distance $d(Cu{-}N^{MeCN})$ = 2.321(3) Å, as expected for a Jahn–Teller d^9 ion (Figure 2b). IR spectroscopy of a solid sample of **2** that was kept under vacuum overnight indicated that the MeCN is weakly bound and readily lost, in accordance with the combustion analysis of the dried product.

The overall coordination environment of the Cu^{II} ion in **2** is best described as a slightly distorted square pyramid with τ_5 = 0.016 (close to the τ_5 value of 0 for an ideal square pyramid).[25] *Trans* angles C^{NHC}-Cu-C^{NHC} and N^{py}-Cu-N^{py} within the basal plane are 168.4(1)° and 169.8(1)°, respectively, and the displacement of the copper ion out of the basal plane is only 0.192(1) Å. Cu–C^{NHC} bonds in **2** (1.907(3) Å and 1.909(3) Å) are clearly shorter than in **1** (1.939(2) Å and 1.946(2) Å), which is consistent with the expectation that the increased electron deficiency of the metal center enhances its interaction with the carbene donors. Cu–C^{NHC} bonds in **2** are at the short end of Cu–C bond lengths of known Cu^{II}–NHC complexes (1.89–2.52 Å).[26] Oxidation of **1** to **2** yields dramatically shortened Cu–N^{py} distances (2.155(2)/2.157(3) Å) that are comparable to those of reported five-coordinate Cu^{II} complexes with chelating NHC-pyridine ligands (2.12–2.21 Å).[26] This leads to a puckered macrocycle with a saddle-like shape and approximate C_2 symmetry in solid **2**, featuring dihedral angles between opposing imidazol-2-ylidene rings and pyridyl rings of 56.1(2)° and 50.1(1)°, respectively. This is reminiscent of the conformations the macrocyclic ligand L adopts in the six-coordinate iron

complexes $[LFe^{II}(NCMe)_2][PF_6]_2$ and $[LFe^{III}(NCMe)_2][PF_6]_3$, as well as in the four-coordinate nickel complex $[LNi^{II}]Br_2$.[15a,d]

SQUID magnetometry of a solid sample of **2** (Figure S15) shows an almost constant $\chi_M T$ value of 0.44 $cm^3 mol^{-1} K$ (corresponding to $\mu_{eff} = 1.88$ μB) over a wide temperature range from 12 to 295 K, as expected for an $S = 1/2$ system with some orbital contributions ($g_{iso} = 2.17$). The X-band EPR spectrum of **2** in MeCN recorded at 298 K displays a nearly isotropic pattern with obvious $^{63/65}Cu$ ($I = 3/2$) and ^{14}N ($I = 1$) hyperfine splitting (Figure 6). The signal could be well simulated with approximately equal g factors ($g_1 = 2.077$, $g_2 = 2.079$, $g_3 = 2.057$),[27] large A^{Cu} (up to 157×10^{-4} cm) and coupling with two ^{14}N atoms ($A^{N}_{av} = 20 \times 10^{-4}$ cm), suggesting that the unpaired spin resides partly on the ligand L. This is corroborated by DFT calculations which, as expected, show that the singly occupied orbital is antibonding and has large $Cu(d_{x^2-y^2})$ character with some $N^{py}(p_y)$ and $C^{NHC}(p_x)$ contributions (Figure S51). Calculated spin densities on Cu and on each pyridine N are 60% and 10%, respectively (Figure 6). The X-band EPR spectrum of **2** measured in frozen MeCN solution at 147 K exhibits a broad rhombic signal with approximate g-values [2.25, 2.12, 2.00] but without resolvable Cu hyperfine splitting (Figure S14). The rhombic character of the g-tensor is indicative of mixing of the d_{z^2} into the $d_{x^2-y^2}$ ground state for C_{2v} symmetry.[28] The paramagnetism of the complex and unfavorable relaxation properties of Cu^{II} ions preclude any NMR spectroscopic characterization.

Copper(III) complex. The Cu^{II} complex **2** can be further oxidized using $[(2,4\text{-}Br_2\text{-}C_6H_3)_3N][SbF_6]$ (a derivative of "Magic Blue" with $E^{o'} = +1.14$ V vs. Fc/Fc^+ in MeCN)[29] as the one-electron oxidant to give diamagnetic $[LCu][PF_6]_2[SbF_6]$ (**3**) as a dark-red crystalline solid in moderate yield (ca. 60%). At room temperature, **3** is stable both in solution and in solid state under inert atmosphere, but it gradually decomposes under aerobic conditions (Figure S7). Its ESI mass spectrum shows major peaks characteristic of **1** and **2**, which possibly arise from the reduction of **3** during the electrospray ionization process.

Dark-red crystals of **3** were obtained by slow diffusion of Et_2O into a saturated MeCN solution of the crude material and were subjected to X-ray diffraction. Two crystallographically independent but similar molecules were found in the asymmetric unit, representing enantiomers in different conformations (Figure S4); one of them is shown in Figure 2. The molecular structure of the trication of **3** in solid state is very similar to that of the dication of **2** (Figure 7 overlay). This suggests a very low reorganization energy for the 1 e^- transfer

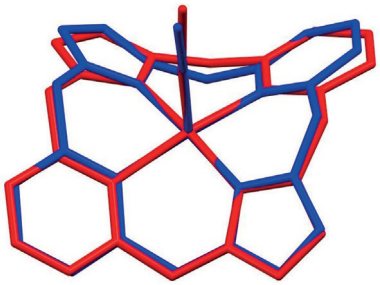

Figure 7. Overlay of the cations of **2** (red) and **3** (blue) with similar conformations.

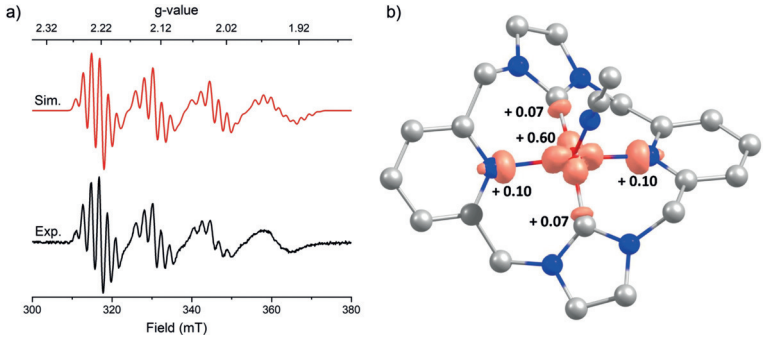

Figure 6. a) EPR spectrum of **2** recorded in MeCN solution at 298 K (black line) and a simulation ($S = {}^1/_2$; $g_1 = 2.077$, $g_2 = 2.079$, $g_3 = 2.057$; $A\_Cu_1 = 424$ MHz, $A\_Cu_2 = 388$ MHz, $A\_Cu_3 = 470$ MHz; $A\_N_1 = 60$ MHz, $A\_N_2 = 65$ MHz, $A\_N_3 = 57$ MHz; full width at half maximum (FWHM) = 13.3 G (red line). b) Overall Löwdin spin population of **2** (isodensity value 0.08 au). Color code: C (gray), N (blue), Cu (red).

when shuttling between **2** and **3**, which is in accordance with the CV data. Oxidation of **2** leads to a significant further shortening of the $Cu\text{–}C^{NHC}$ (1.875(4)/1.880(4) Å) and $Cu\text{–}N^{py}$ bonds (1.972(3)–1.974(3) Å) in **3** (Table 1), reflecting the removal of an electron from the antibonding $d_{x^2-y^2}$ orbital. The $Cu\text{–}C^{NHC}$ bond lengths in **3** are comparable with those reported recently for the tricationic tetra(NHC)-Cu^{III} complex $[L^{NHC}Cu][OTf]_3$ (1.879–1.884 Å; Figure 1b).[11] The apical $Cu\text{–}N^{MeCN}$ distance of 2.325(4) Å in **3** is almost unchanged from **2** (2.321(3) Å), but the MeCN ligation is more bent (angle $Cu\text{-}N^{MeCN}\text{-}C^{MeCN}$: 160.7(4)° in **3** vs. 173.8(3)° in **2**). The invariant $Cu\text{–}N^{MeCN}$ bond length suggests that the interaction with the apical MeCN ligand is electronically insignificant, and that electronic changes upon

Table 1: Selected atom distances (Å) and angles (°) of **1**, **2**, and **3** obtained from the crystallographic analyses.

Complexes	Cu–C1	Cu–C11	Cu–N1	Cu–N4	Cu–N7	C1-Cu-C11	N1-Cu-N4	C21-N7-Cu
1	1.939(2)	1.946(2)	2.706(2)	2.496(2)		169.62(8)	164.49(5)	
2	1.909(3)	1.907(3)	2.157(3)	2.155(2)	2.321(3)	168.42(13)	169.83(9)	173.8(3)
3	1.880(4)	1.875(4)	1.974(3)	1.972(3)	2.325(4)	173.36(17)	173.14(13)	160.7(4)
3′[a]	1.868(4)	1.868(4)	1.964(3)	1.974(3)	2.315(4)	172.55(17)	172.25(13)	165.9(4)

[a] The conformational enantiomer of **3** in the crystal unit.

oxidation of **2** to **3** occur within the basal plane. Similar to **2**, the weakness of the apical interaction leads to facile removal of the MeCN when **3** is kept under vacuum, which is evidenced by IR spectroscopy and elemental analysis of a dried sample (Figure S8).

The diamagnetism of **3** is reflected by sharp ^{1}H NMR signals in the normal range (0–9 ppm in [D$_3$]MeCN). All peaks of **3** are dramatically shifted to lower field compared to those of **1**, in line with the electron-deficient nature of the Cu^{III} center. In contrast to **1**, however, the CH$_2$ linkers of the macrocyclic ligand show an AB spin system at room temperature where the central peaks are no longer resolved but the small outer peaks are still visible; the central peak evolves into two strongly coupled doublets ($J_{ab} = 17.0$ Hz, $\nu_{ab}/J_{ab} < 1$) at lower temperatures (Figure 8; Figure S46; coalescence

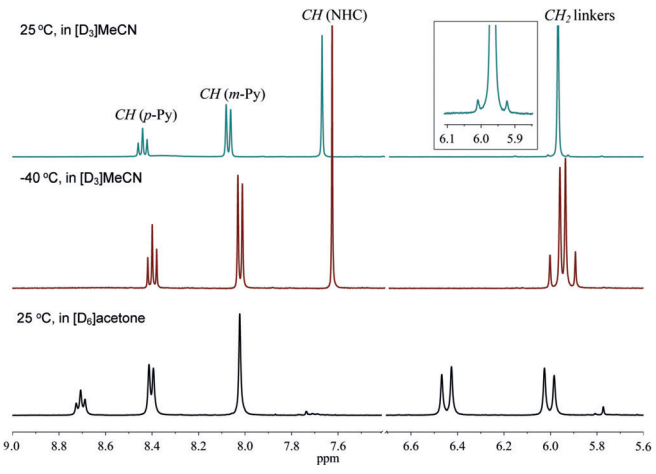

Figure 8. ^{1}H NMR spectra of complex **3** in [D$_3$]MeCN (top, 25 °C; middle, −40 °C) and [D$_6$]acetone (bottom, 25 °C). Only regions 5.6–6.7 ppm and 7.4–9.0 ppm are shown for clarity. Inset: magnified range 5.8–6.1 ppm for **3** in [D$_3$]MeCN at 25 °C.

temperature $T_c = 4$ °C). In [D$_6$]acetone, the CH$_2$ linkers give rise to two apparent doublets at room temperature ($J_{ab} =$ 16.8 Hz, $\nu_{ab}/J_{ab} = 4.3$; Figure 8). This indicates a more rigid macrocyclic skeleton in **3** compared to **1**. Any dynamics of the puckered conformation in solution are slow on the NMR timescale, as was observed for [LNi^{II}]Br$_2$,[15a] which also reflects the shortened Cu–N/C bonds. As a consequence of the temperature limitation of the solvent and the instability of **3** at a higher temperature (it decomposes quickly at 50 °C in [D$_6$]acetone), attempts to observe dynamic behavior and to derive reliable activation parameters from NMR spectroscopy were unsuccessful. The substantial high-field shift of the ^{15}N NMR resonance for the N^{py} atoms in complex **3** (−171.0 ppm) compared to −77.6 ppm for [H$_2$L][PF$_6$]$_2$ and −67.5 ppm for **1** indicates a strong interaction of the pyridine donors with the oxidized metal ion. Remarkably, the ^{13}C NMR signal for the imidazol-2-ylidene C2 atoms of **3** is shifted to a rather high-field value (151.8 ppm), which is similar to what has been reported for the macrocyclic tetra(NHC) ligated Cu^{III} (149.4 ppm) and Au^{III} complexes (ca. 146 ppm).[11,30] The diffusion coefficient of **3** ($D_{298K} = 9.14 \times 10^{-10}$ m^2 s^{-1}, determined by ^{1}H DOSY) is similar to those of **1** and the imidazolium salt [H$_2$L][PF$_6$]$_2$, suggesting that the mononuclear structure is retained in solution.

Oxidation State Assignments. The redox non-innocent character of many macrocyclic ligands used in previously reported formal Cu^{III} complexes, such as carbaporphyrins and corroles (Figure 1 a),[4e,31] lends some ambiguity to the metal oxidation state assignments. Hence, the electronic structure of **3** was examined computationally as well as by XAS. Ground state DFT calculations suggest that **3** is best described as a closed shell singlet Cu^{III} system with the triplet state being 25.2 kcal mol^{-1} higher in energy; broken-symmetry calculations revealed the antiferromagnetically coupled open-shell $S = 0$ state to be even more unfavorable (Table 2; Table S8).

Table 2: Comparison of the selected bond distances (Å) and relative single-point energies (kcal mol^{-1}) obtained from the optimized geometries of **3** at different spin states (closed shell singlet state and triplet state); BS (broken-symmetry state) (1,1) at +26.6 kcal mol^{-1} (Supporting Information).

Complex	**3** ($S = 0$)	**3** ($S = 1$)	**3** (Exp.)
Cu–C	1.8872/1.8874	1.9106/1.9104	1.867(4)–1.880(3)
Cu–N$_{Py}$	2.0204/2.0201	2.2058/2.2061	1.965(3)–1.974(3)
Cu–N$_{MeCN}$	2.3293	2.1730	2.315(3)/2.326(4)
E_{rel}	0	25.2	–

Furthermore, both the calculated Cu–N/C bond distances after geometry optimization (Table 2), and the calculated UV/Vis spectrum (Figure S50) match the experimental data best for the closed shell singlet Cu^{III} configuration. The lowest unoccupied molecular orbital (LUMO) of **3** is antibonding with significant Cu($d_{x^2-y^2}$) character, which is consistent with the removal of one electron from the singly occupied molecular orbital (SOMO) of **2**, whereas the highest occupied molecular orbital (HOMO) to HOMO-8 of **3** are mainly ligand-centered orbitals with less than 4 % percent of Cu(d) contributions (Figure S52, Table S9).

To corroborate the oxidation state assignments of the copper complexes of L reported herein, and specifically the Cu^{III} character of **3**, Cu Kβ high-energy-resolution fluorescence detection (HERFD) XAS was performed for the series of complexes **1**–**3**. This detection technique records the Cu K-edge absorption spectrum by monitoring a 3p→1s fluorescence signal with a large, high-resolution emission spectrometer (ca. 1 eV resolution). The resultant narrower absorption linewidth is determined by the longer 3p core–hole lifetime, as opposed to the shorter 1s core–hole lifetime in traditional XAS measurements.

The Cu Kβ HERFD-XAS of **1** reveals two sharp features at 8981.8 and 8984.8 eV (Figure 9). These lowest energy, intense transitions beginning at approximately 8982 eV are consistent with the d^{10} electronic configuration of Cu^I, where the first Cu K-edge transitions correspond to dipole-allowed 1s→4p transitions. The reduced local symmetry of the Cu^I center (where the z axis is along the C^{NHC}–Cu–C^{NHC} direction) lifts the degeneracy of the Cu 4p orbital energies. The first peak is assigned as the Cu 1s→4p$_y$ with predominant C^{NHC}(p$_y$) and Cu(p$_y$) character from an unoccupied C–Cu π-like orbital (Figure S53). The higher energy feature corre-

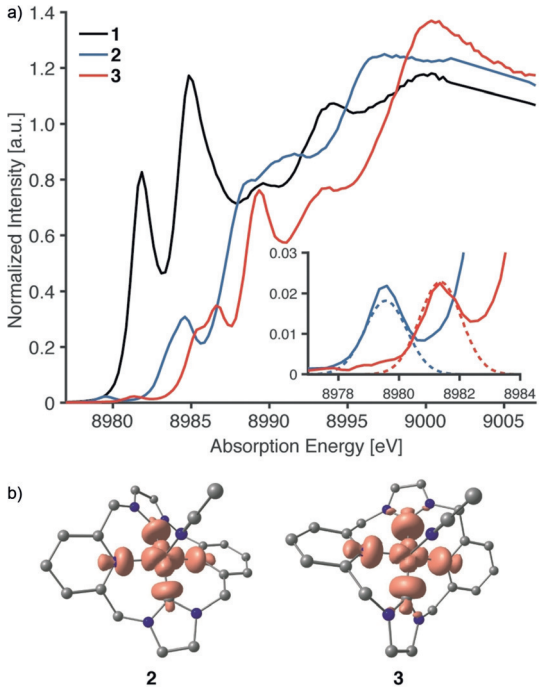

Figure 9. a) Cu Kβ HERFD-XAS of **1**–**3** (up, solid lines). Inset: TD-DFT-calculated pre-edge spectra of **2** and **3** (dashed lines). Each calculated pre-edge consists of a single transition, broadened by 1.4 eV (FWHM). b) The transition difference density plots for each pre-edge transition of **2** and **3** (bottom) are shown with isodensity value = 0.003 au. Color code: C (gray), N (blue), Cu (red), hydrogen atoms omitted. Calculations shifted by +188.55 eV.

sponds to the Cu 1s→4p$_x$ transitions of the orthogonal C–Cu π-like interaction, with contributions from the pyridine σ (p$_x$) orbitals (Figure S53).

The Cu Kβ HERFD-XAS of **2** is dramatically different from the spectrum of **1** (Figure 9); the intense dipole-allowed transitions are gone in the spectrum of **2** and the rising edge is shifted to higher energy, reflecting a deeper 1s electron binding energy of the higher oxidation state. At 8979.5 eV, a weak pre-edge feature is observed corresponding to a dipole-forbidden 1s→3d transition into the single d electron–hole of the d^9 Cu^{II} center.[6b,32]

The most oxidized complex, **3**, possesses the highest energy absorption edge—indicative of Cu^{III}. A weak pre-edge feature is observed at 8981.3 eV for **3**, which is approximately 1.8 eV higher than the established Cu^{II} pre-edge energy of **2** and consistent with previous reports for Cu^{III} complexes.[6b] Furthermore, the observed shifts in the whiteline energies for **1**, **2**, and **3**, at approximately 8994, 8996.5, and 9000 eV, respectively, are consistent with the increasing copper oxidation state.

TD-DFT calculations of the Cu pre-edge features of **2** and **3** each show a single transition into a predominantly d$_{x^2-y^2}$ unoccupied orbital, as evidenced by the transition difference density plots (Figure 9). These calculations (using the PBE0 functional and def2-TZVP basis set) reproduce the relative energies of the pre-edges well, with the Cu^{III} pre-edge predicted to be 1.81 eV higher in energy than the Cu^{II} analogue.

Conclusion

In this study, we have shown that the bis(NHC)-bis(pyridine) hybrid macrocycle L is capable of accommodating copper in three sequential oxidation states, from +I to +III. Structural characterization of the complexes [LCu]$^{+/2+/3+}$ (**1**–**3**) evidences hemilability of the two pyridine donors, which allows the ligand to adapt to the very different stereoelectronic requirements and coordination preferences of Cu^{I} versus Cu^{II}/Cu^{III} while retaining the linear C^{NHC}-Cu-C^{NHC} arrangement throughout the series. In the oxidized species **2** and **3**, the two pyridine donors swing in to provide the additional two equatorial donors that establish the square planar environment required for hosting Cu^{II} and Cu^{III} ions. While NHC-Cu^{I} complexes are abundant, Cu^{II} complexes with NHC ligation are rare and their redox chemistry is generally associated with decomposition or major structural changes. A recently reported Cu^{III} complex of a tetra(NHC) macrocycle has a strongly destabilized Cu(d$_{x^2-y^2}$) orbital and lacks the ligand hemilability that is required to enable reduction to the Cu^{I} state.[11] Hence the present system is unique in that it allows for accessing all three copper oxidation states with little structural reorganization and within a useful potential window for the redox interconversions, which occur at $E_{1/2} = -0.45$ V and +0.82 V (vs. Fc/Fc$^+$). An interesting aspect for future reactivity studies is that the addition of two electrons upon reduction of **3** to **1** also exposes two basic pyridine N atoms, suggesting that the electron transfer might be coupled with proton transfer.

The electronic structure of formal Cu^{III} complexes is a matter of active investigation and debate because, in many reported cases, ligand non-innocence has to be considered.[5,31] For instance, [Cu(CF$_3$)$_4$]$^-$ and related systems have recently been described as having a 3d^{10} ground state electronic configuration because of an inverted ligand field (that is, Cu^{I} character with the LUMO having predominantly trifluoromethyl character).[5d] In contrast, X-ray spectroscopic studies on the present series of [LCu]$^{+/2+/3+}$ complexes have revealed textbook examples of XAS signatures for Cu^{I}, Cu^{II}, and Cu^{III}, in **1**, **2**, and **3**, respectively. These findings are also in accordance with the other data and DFT results, and they indicate that **3** is a genuine Cu^{III} species. This is in line with NHC ligands being extremely strong σ-donor ligands that are largely redox innocent and are capable of supporting high oxidation state 3d metal complexes.[8]

Acknowledgements

Y.L. is grateful to the Alexander von Humboldt Foundation for a postdoctoral fellowship, and S.G.R. has been supported by the International PhD program *Catalysis for Sustainable Synthesis* (CaSuS). S.G.R. and Y.L. thank R. Schöne for technical support with NMR measurements, and Y.L. thanks Dr. A. C. Stückl for EPR measurements. G.C. and S.D. acknowledge financial support from the Max Planck Society. SSRL is acknowledged for allocation of beamtime. SSRL is supported by the U.S. Department of Energy, Office of

Science, Office of Basic Energy Sciences under Contract No. DE-AC02-76SF00515.

Conflict of interest

The authors declare no conflict of interest.

Keywords: copper(III) · macrocyclic ligands · N-heterocyclic carbenes · oxidation states · X-ray absorption spectroscopy

How to cite: *Angew. Chem. Int. Ed.* **2020**, *59*, 5696–5705
Angew. Chem. **2020**, *132*, 5745–5754

[1] a) E. Nakamura, S. Mori, *Angew. Chem. Int. Ed.* **2000**, *39*, 3750; *Angew. Chem.* **2000**, *112*, 3902; b) A. J. Hickman, M. S. Sanford, *Nature* **2012**, *484*, 177; c) S. E. Allen, R. R. Walvoord, R. Padilla-Salinas, M. C. Kozlowski, *Chem. Rev.* **2013**, *113*, 6234; d) A. Casitas, X. Ribas, *Chem. Sci.* **2013**, *4*, 2301; e) B. Liu, W.-Z. Chen, *Chin. J. Inorg. Chem.* **2014**, *30*, 20.

[2] a) E. I. Solomon, D. E. Heppner, E. M. Johnston, J. W. Ginsbach, J. Cirera, M. Qayyum, M. T. Kieber-Emmons, C. H. Kjaergaard, R. G. Hadt, L. Tian, *Chem. Rev.* **2014**, *114*, 3659; b) W. Keown, J. B. Gary, T. D. P. Stack, *J. Biol. Inorg. Chem.* **2017**, *22*, 289; c) C. E. Elwell, N. L. Gagnon, B. D. Neisen, D. Dhar, A. D. Spaeth, G. M. Yee, W. B. Tolman, *Chem. Rev.* **2017**, *117*, 2059; d) K. V. N. Esguerra, J. P. Lumb, *Synthesis* **2019**, *51*, 334.

[3] R. Santo, R. Miyamoto, R. Tanaka, T. Nishioka, K. Sato, K. Toyota, M. Obata, S. Yano, I. Kinoshita, A. Ichimura, T. Takui, *Angew. Chem. Int. Ed.* **2006**, *45*, 7611; *Angew. Chem.* **2006**, *118*, 7773.

[4] a) X. Ribas, D. A. Jackson, B. Donnadieu, J. Mahía, T. Parella, R. Xifra, B. Hedman, K. O. Hodgson, A. Llobet, T. D. P. Stack, *Angew. Chem. Int. Ed.* **2002**, *41*, 2991; *Angew. Chem.* **2002**, *114*, 3117; b) B. Yao, D. X. Wang, Z. T. Huang, M. X. Wang, *Chem. Commun.* **2009**, 2899; c) H. Furuta, H. Maeda, A. Osuka, *J. Am. Chem. Soc.* **2000**, *122*, 803; d) H. Maeda, A. Osuka, H. Furuta, *J. Am. Chem. Soc.* **2003**, *125*, 15690; e) M. Pawlicki, I. Kanska, L. Latos-Grazynski, *Inorg. Chem.* **2007**, *46*, 6575; f) H. Zhang, B. Yao, L. Zhao, D. X. Wang, B. Q. Xu, M. X. Wang, *J. Am. Chem. Soc.* **2014**, *136*, 6326; g) B. Adinarayana, A. P. Thomas, C. H. Suresh, A. Srinivasan, *Angew. Chem. Int. Ed.* **2015**, *54*, 10478; *Angew. Chem.* **2015**, *127*, 10624; h) X. S. Ke, Y. Hong, P. Tu, Q. He, V. M. Lynch, D. Kim, J. L. Sessler, *J. Am. Chem. Soc.* **2017**, *139*, 15232; i) Y. K. Maurya, K. Noda, K. Yamasumi, S. Mori, T. Uchiyama, K. Kamitani, T. Hirai, K. Ninomiya, M. Nishibori, Y. Hori, Y. Shiota, K. Yoshizawa, M. Ishida, H. Furuta, *J. Am. Chem. Soc.* **2018**, *140*, 6883.

[5] a) D. Naumann, T. Roy, K. Tebbe, W. Crump, *Angew. Chem. Int. Ed. Engl.* **1993**, *32*, 1482; *Angew. Chem.* **1993**, *105*, 1555; b) J. P. Snyder, *Angew. Chem. Int. Ed. Engl.* **1995**, *34*, 80; *Angew. Chem.* **1995**, *107*, 112; c) N. C. Tomson, K. D. Williams, X. Dai, S. Sproules, S. DeBeer, T. H. Warren, K. Wieghardt, *Chem. Sci.* **2015**, *6*, 2474; d) R. C. Walroth, J. T. Lukens, S. N. MacMillan, K. D. Finkelstein, K. M. Lancaster, *J. Am. Chem. Soc.* **2016**, *138*, 1922.

[6] a) C. Krebs, T. Glaser, E. Bill, T. Weyhermüller, W. Meyer-Klaucke, K. Wieghardt, *Angew. Chem. Int. Ed.* **1999**, *38*, 359; *Angew. Chem.* **1999**, *111*, 370; b) J. L. DuBois, P. Mukherjee, T. D. P. Stack, B. Hedman, E. I. Solomon, K. O. Hodgson, *J. Am. Chem. Soc.* **2000**, *122*, 5775; c) W. Sinha, M. G. Sommer, N. Deibel, F. Ehret, M. Bauer, B. Sarkar, S. Kar, *Angew. Chem. Int. Ed.* **2015**, *54*, 13769; *Angew. Chem.* **2015**, *127*, 13973.

[7] a) F. E. Hahn, M. C. Jahnke, *Angew. Chem. Int. Ed.* **2008**, *47*, 3122; *Angew. Chem.* **2008**, *120*, 3166; b) M. N. Hopkinson, C. Richter, M. Schedler, F. Glorius, *Nature* **2014**, *510*, 485; c) V. Charra, P. de Frémont, P. Braunstein, *Coord. Chem. Rev.* **2017**, *341*, 53; d) E. Peris, *Chem. Rev.* **2018**, *118*, 9988.

[8] J. Cheng, L. Wang, P. Wang, L. Deng, *Chem. Rev.* **2018**, *118*, 9930.

[9] A. J. Arduengo III, H. V. R. Dias, J. C. Calabrese, F. Davidson, *Organometallics* **1993**, *12*, 3405.

[10] a) J. C. Y. Lin, R. T. W. Huang, C. S. Lee, A. Bhattacharyya, W. S. Hwang, I. J. B. Lin, *Chem. Rev.* **2009**, *109*, 3561; b) F. Lazreg, F. Nahra, C. S. J. Cazin, *Coord. Chem. Rev.* **2015**, *293–294*, 48; c) A. A. Danopoulos, T. Simler, P. Braunstein, *Chem. Rev.* **2019**, *119*, 3730.

[11] Z. S. Ghavami, M. R. Anneser, F. Kaiser, P. J. Altmann, B. J. Hofmann, J. F. Schlagintweit, G. Grivani, F. E. Kühn, *Chem. Sci.* **2018**, *9*, 8307.

[12] a) A. O. Larsen, W. Leu, C. N. Oberhuber, J. E. Campbell, A. H. Hoveyda, *J. Am. Chem. Soc.* **2004**, *126*, 11130; b) P. L. Arnold, M. Rodden, K. M. Davis, A. C. Scarisbrick, A. J. Blake, C. Wilson, *Chem. Commun.* **2004**, 1612; c) J. Yun, D. Kimb, H. Yun, *Chem. Commun.* **2005**, 5181; d) C. Y. Legault, C. Kendall, A. B. Charette, *Chem. Commun.* **2005**, 3826; e) B. Liu, B. Liu, Y. Zhou, W. Chen, *Organometallics* **2010**, *29*, 1457; f) Q. Liu, M. Shi, Z. Wang, S. Liu, S. Ge, Y. Zang, X. Wang, J. Guo, *Polyhedron* **2010**, *29*, 2121; g) D. I. Bezuidenhout, G. Kleinhans, G. Guisado-Barrios, D. C. Liles, G. Ung, G. Bertrand, *Chem. Commun.* **2014**, *50*, 2431; h) B. R. M. Lake, C. E. Willans, *Organometallics* **2014**, *33*, 2027; i) D. J. O'Hearn, R. D. Singer, *Organometallics* **2017**, *36*, 3175; j) S. A. Lin, Y. Liu, S. Peng, S. Liu, *J. Organomet. Chem.* **2018**, *859*, 52.

[13] a) X. Hu, I. Castro-Rodriguez, K. Meyer, *J. Am. Chem. Soc.* **2003**, *125*, 12237; b) J. M. Smith, J. R. Long, *Inorg. Chem.* **2010**, *49*, 11223.

[14] a) B. Lin, P. Kang, T. D. P. Stack, *Organometallics* **2010**, *29*, 3683; b) B. R. M. Lake, A. Ariafard, C. E. Willans, *Chem. Eur. J.* **2014**, *20*, 12729; c) T. J. Williams, J. T. W. Bray, B. R. M. Lake, C. E. Willans, N. A. Rajabi, A. Ariafard, C. Manzini, F. Bellina, A. C. Whitwood, I. J. S. Fairlamb, *Organometallics* **2015**, *34*, 3497; d) Y. Younesi, B. Nasiri, R. BabaAhmadi, C. E. Willans, I. J. S. Fairlamb, A. Ariafard, *Chem. Commun.* **2016**, *52*, 5057.

[15] a) M. V. Baker, B. W. Skelton, A. H. White, C. C. Williams, *Organometallics* **2002**, *21*, 2674; b) H. M. Lee, C. Lee, P. Cheng, *Curr. Org. Chem.* **2007**, *11*, 1491; c) B. Liu, Q. Xia, W. Chen, *Angew. Chem. Int. Ed.* **2009**, *48*, 5513; *Angew. Chem.* **2009**, *121*, 5621; d) I. Klawitter, M. R. Anneser, S. Dechert, S. Meyer, S. Demeshko, S. Haslinger, A. Pöthig, F. E. Kühn, F. Meyer, *Organometallics* **2015**, *34*, 2819.

[16] J. C. Garrison, R. S. Simons, J. M. Talley, C. Wesdemiotis, C. A. Tessier, W. J. Youngs, *Organometallics* **2001**, *20*, 1276.

[17] P. J. Barnard, M. V. Baker, S. J. Berners-Price, B. W. Skelton, A. H. White, *Dalton Trans.* **2004**, 1038.

[18] B. R. M. Lake, E. K. Bullough, T. J. Williams, A. C. Whitwood, M. A. Little, C. E. Willans, *Chem. Commun.* **2012**, *48*, 4887.

[19] a) S. Diez-González, E. D. Stevens, N. M. Scott, J. L. Petersen, S. P. Nolan, *Chem. Eur. J.* **2008**, *14*, 158; b) S. Diez-Gonzalez, N. M. Scott, S. P. Nolan, *Organometallics* **2006**, *25*, 2355.

[20] R. McKie, J. A. Murphy, S. R. Park, M. D. Spicer, S. Zhou, *Angew. Chem. Int. Ed.* **2007**, *46*, 6525; *Angew. Chem.* **2007**, *119*, 6645.

[21] a) R. E. Andrew, C. M. Storey, A. B. Chaplin, *Dalton Trans.* **2016**, *45*, 8937; b) D. Domyati, S. L. Hope, R. Latifi, M. D. Hearns, L. Tahsini, *Inorg. Chem.* **2016**, *55*, 11685; c) D. Domyati, R. Latifi, L. Tahsini, *J. Organomet. Chem.* **2018**, *860*, 98.

[22] a) K. Riener, A. Pöthig, M. Cokoja, W. A. Herrmann, F. E. Kühn, *Acta Crystallogr. Sect. C* **2015**, *71*, 643; b) B. Liu, X. Ma, F. Wu, W. Chen, *Dalton Trans.* **2015**, *44*, 1836.
[23] J. C. Garrison, R. S. Simons, C. A. Tessier, W. J. Youngs, *J. Organomet. Chem.* **2003**, *673*, 1.
[24] A. Raba, M. Cokoja, S. Ewald, K. Riener, E. Herdtweck, A. Pöthig, W. A. Herrmann, F. E. Kühn, *Organometallics* **2012**, *31*, 2793.
[25] L. Yang, D. R. Powell, R. P. Houser, *Dalton Trans.* **2007**, 955.
[26] Based on a search of the Cambridge Structural Database (CSD, 2019). "The Cambridge Structural Database": C. R. Groom, I. G. Bruno, M. P. Lightfoot, S. C. Ward, *Acta Crystallogr. Sect. B* **2016**, *72*, 171.
[27] Slow tumbling of the molecules may be the reason that the signal is not strictly isotropic, see: D. M. Murphy in *Metal Oxide Catalysis* (Eds.: S. D. Jackson, J. S. J. Hargreaves), Wiley-VCH, Weinheim, **2009**.
[28] B. J. Hathaway, D. E. Billing, *Coord. Chem. Rev.* **1970**, *5*, 143.
[29] N. G. Connelly, W. E. Geiger, *Chem. Rev.* **1996**, *96*, 877.
[30] a) A. H. Mageed, B. W. Skelton, M. V. Baker, *Dalton Trans.* **2017**, *46*, 7844; b) Z. Lu, S. A. Cramer, D. M. Jenkins, *Chem. Sci.* **2012**, *3*, 3081.
[31] a) A. Ghosh, T. Wondimagegn, A. B. J. Parusel, *J. Am. Chem. Soc.* **2000**, *122*, 5100; b) A. Ghosh, E. Steene, *J. Biol. Inorg. Chem.* **2001**, *6*, 739; c) I. Luobeznova, L. Simkhovich, I. Goldberg, Z. Gross, *Eur. J. Inorg. Chem.* **2004**, 1724; d) A. Ghosh, *Chem. Rev.* **2017**, *117*, 3798; e) S. Ganguly, A. Ghosh, *Acc. Chem. Res.* **2019**, *52*, 2003.
[32] L. S. Kau, D. J. Spira-Solomon, J. E. Penner-Hahn, K. O. Hodgson, E. I. Solomon, *J. Am. Chem. Soc.* **1987**, *109*, 6433.

Manuscript received: October 5, 2019
Accepted manuscript online: November 25, 2019
Version of record online: January 24, 2020

